JOURNAL OF COMPUTATIONAL PHYSICS 104, 173–184 (1993)

Numerical Methods for Two-Dimensional Analysis of Electrical Breakdown in a Non-uniform Gap

K. RAMAKRISHNA*

Materials Science, Technology Products, IBM Corporation, Endicott, New York 13760-8003

AND

I. M. COHEN AND P. S. AYYASWAMY

Department of Mechanical Engineering and Applied Mechanics, School of Engineering and Applied Science, University of Pennsylvania, Philadelphia, Pennsylvania 19104-6315

Received May 10, 1990; revised March 3, 1992

A finite difference procedure used to analyze the two-dimensional evolution of the charged particle densities and electrostatic potential during the initial stages of electrical breakdown between a wire and a plane is described. The diffusion flux equations for the charged particle densities and Poisson's equation for the electrostatic potential constitute a set of coupled, two-dimensional, time dependent, nonlinear equations that govern the breakdown phenomena. In this paper, we have solved the problem by two different procedures: (a) a finite difference method that combines upwind difference scheme (UDS) for drift terms, central difference scheme (CDS) for the diffusion terms, and implicit time integration; and (b) a method that combines CDS for drift terms, CDS for the diffusion terms, and implicit time integration. In each case, Crank–Nicolson time integration has also been tried. It is concluded that method (a) is most suitable for discharge breakdown problems.

I. INTRODUCTION

Electrical discharges may be initiated by high voltage breakdown of the gas between two electrodes. For very low current densities and where the space charge effects are negligible, it is possible to obtain analytical solutions of discharge breakdown models in plane parallel geometries. See, for example, Meek and Craggs [1]. However, at higher voltages and currents, the space charge effects and the electric field dependence of the ionization coefficients render the governing equations nonlinear, and numerical procedures have to be employed. The existing numerical studies in this regard are mainly concerned with the growth of the discharge in a parallel plane geometry [2–5], using the method of characteristics. Davies *et al.* [6] have attempted to obtain two-dimensional solutions of discharge growth in a non-uniform gap by employing the method of characteristics and variable grid for the particle conservation equations. The potential has been computed by a fast Fourier transform algorithm in two stages with two types of uniform grid. However, convergence difficulties and vast computer time and storage requirements have been reported.

Finite difference methods have been used to describe one-dimensional models of breakdown [7–10]. Morrow and his co-workers [8–10] have applied the flux corrected transport (FCT) algorithm, originally proposed by Boris and Book [11], to discharge problems. These are explicit upwind methods. Based on a comparison of several explicit methods, including the FCT method and its variants, applied to one-dimensional discharge problems [8], it is concluded that full flux correction of the FCT method with a peak preserving method yields best results. Extension of this method to nonuniform meshes and to diffusion is given by Morrow and Cram [10]. A recent review and extension of the FCT algorithm for fluid mechanical problems has been provided by Munz [12]. He has compared FCT method with the monotonic upstream-centered scheme for conservation law (MUSCL), which is particularly suited for such problems. It may be noted here that the FCT methods are explicit in nature and are restricted by the limitations imposed by the stability criteria and numerical diffusion [8]. Novak and Bartnikas [13] have used a finite element program for the two-dimensional parallel plane problem. An excellent summary of the numerical methods used in the breakdown problem is given by Davies [14].

In this paper, we have numerically examined the two-dimensional model of electrical breakdown in a non-uniform gap by finite difference methods. Our examination has been carried out in the following manner shown in Table I.

* Author to whom correspondence should be addressed.

0021-9991/93 $5.00

TABLE I

Numerical Procedures for the Particle Conservation Equations

	Drift terms	Diffusion terms	Time integration
Method (A)	UDS	CDS	Implicit
Method (B)	CDS	CDS	Implicit
Method (C)	UDS	CDS	Crank–Nicolson
Method (D)	CDS	CDS	Crank–Nicolson

Note. CDS, central difference scheme, UDS, upwind difference scheme.

In all of the methods central differences are used for Poisson's equation. The algebraic equations are solved by the line-by-line method along with the Thomas algorithm. A two-tier block iterative method and underrelaxation have been employed for the solution of the algebraic equations. Extensive numerical experimentation was necessary to determine the accuracy of these methods. Comparisons have been made among the results of various methods. We conclude that methods (A) and (C) are suitable for discharge breakdown problems as they provide stability of the numerical solutions. Since method (A) requires less computational time and storage, it is to be preferred. In methods (B) and (D), the central differences for the drift terms gave rise to numerical oscillations and negative number densities after an initial period.

II. GOVERNING EQUATIONS, INITIAL AND BOUNDARY CONDITIONS

Consider a slightly ionized, collision-dominated plasma which is adequately described by the continuum (diffusion flux) conservation equations. The diffusion flux equations are given by

$$\frac{\partial N_e}{\partial t'} + \nabla' \cdot \Gamma_e = P(N_e) - R(N_e) \qquad \text{for electrons} \quad (1)$$

and the self-consistent electrostatic potential, V, is given by Gauss' law as

$$\nabla'^2 V = -\frac{e}{\varepsilon_0}(N_+ - N_e), \quad (2)$$

where

$$\Gamma_e = -\frac{\mu_e}{e}[\nabla p_e + eN_e\mathbf{E}']; \qquad p_e = kT'_eN_e \quad (3)$$

and the electric field is

$$\mathbf{E}' = \nabla' V. \quad (4)$$

An equation similar to Eq. (1) can be written for the positive ions. In the above equations, N is number density, P is volumetric production (ionization) rate, R is volumetric recombination rate, Γ is particle current density, μ is the charged particle mobility, and e is the magnitude of charge on a single electron. Diffusion coefficients have been replaced by $kT'\mu/e$ through Einstein's relation.

Assumptions employed in the derivation of the equations and the details of the modeling of the ionization and recombination mechanisms are discussed in [15, 17]. In summary, the major source of charged particles is ionization by electron impact (Townsend's mechanism) in the volume of the discharge. Thermal ionization and recombination are also considered, but their contribution is found to be negligible in this case. Electrodes are assumed to be absorbing surfaces.

For the hyperboloid wire-to-plane gap, it is appropriate to use prolate spheroidal coordinates [16] as shown in Fig. 1,

$$\begin{aligned} x &= \mathbf{a} \sinh u \sin v \cos \phi \\ y &= \mathbf{a} \sinh u \sin v \sin \phi \\ z &= \mathbf{a} \cosh u \cos v, \end{aligned} \quad (5)$$

where x, y, z are the Cartesian coordinates and u, v, ϕ are the prolate spheroidal coordinates. Here, $u =$ constant are prolate spheroids, $v =$ constant are hyperboloids, $\phi =$

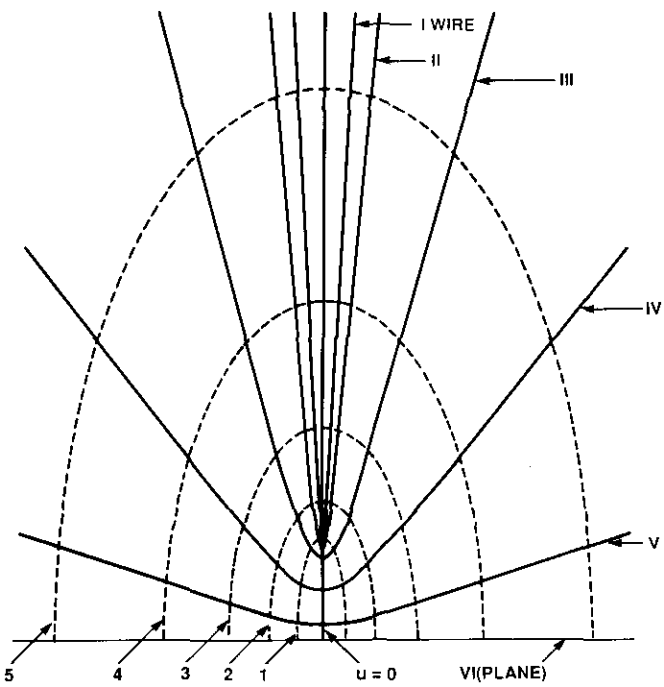

FIG. 1. Schematic diagram of prolate spheroidal coordinate system for the study of electrical breakdown between a wire and a plane. Legend: 1. $u = 0.5$; 2. $u = 1.0$; 3. $u = 1.5$; 4. $u = 2.0$; 5. $u = 2.5$; I. $v = 0.1$; II. $v = 0.1785$; III. $v = 0.5$; IV. $v = 1.0$; V. $v = 1.4$; VI. $v = \pi/2$ (plane).

constant are half-planes, and **a** is the semi-focal distance. In these coordinates, the wire electrode corresponds to $v = v_w$, which is non-zero and needs to be specified, and the wand to $v = \pi/2$. $u = 0$ is the centerline of the discharge and $u \to \infty$ is into the ambient.

Normalization of the governing differential equations, boundary, and initial conditions are discussed in detail in [15]. Only the final forms of the equations are given below:

(a) *Electrons*:

$$\frac{\partial n_e}{\partial t} + \frac{F_e}{[\sinh^2 u + \sin^2 v]}\left[\frac{1}{\sinh u}\frac{\partial}{\partial u}\left[\sinh u\, n_e \frac{\partial \psi}{\partial u}\right] + \frac{1}{\sin v}\frac{\partial}{\partial v}\left[\sin v\, n_e \frac{\partial \psi}{\partial v}\right]\right] = \frac{F_e T_e}{[\sinh^2 u + \sin^2 v]}\left[\frac{1}{\sinh u}\frac{\partial}{\partial u}\left[\sinh u \frac{\partial n_e}{\partial u}\right] + \frac{1}{\sin v}\frac{\partial}{\partial v}\left[\sin v \frac{\partial n_e}{\partial v}\right]\right] + e^{-\mathbf{B}_i/E} n_e E + C_1 C_2 n_e T_e^{-3} e^{-\psi_i/T_e} - C_1 T_e^{-9/2} n_e^2 n_+ \quad (6)$$

and

(b) *Electrostatic Potential*:

$$\frac{1}{[\sinh^2 u + \sin^2 v]}\left[\frac{1}{\sinh u}\frac{\partial}{\partial u}\left[\sinh u \frac{\partial \psi}{\partial u}\right] + \frac{1}{\sin v}\frac{\partial}{\partial v}\left[\sin v \frac{\partial \psi}{\partial v}\right]\right] = \frac{a^2}{d^2}(n_e - n_+), \quad (7)$$

where

$$n = \frac{N}{N_R}, \qquad \psi = \frac{V}{V_R},$$

$$T = \frac{T'}{T'_\infty}, \qquad E = \frac{E'}{E'_R}$$

$$N_R = \frac{kT'_\infty \varepsilon_0}{e^2 d^2}, \qquad V_R = \frac{kT'_\infty}{e}, \qquad E'_R = \frac{V_R}{d}$$

$$t = \frac{t'}{t'_R}, \qquad t'_R = \frac{1}{A_i p \mu_e E'_R}$$

$$F_e = \frac{\mu_e V_R t'_R}{a^2}$$

$$C_1 = 1.09 \times 10^{-20} N_R^2 T'^{-9/2}_\infty t'_R$$

$$C_2 = \frac{4.8186 \times 10^{21} N_n g_i T'^{3/2}_\infty}{N_R^2 g_n}$$

and N_n is the neutral particle density.

The dimensionless form of the positive ion equation is similar to Eq. (6) with the use of ion transport coefficients and the change of sign of the drift terms. Limiting forms of the governing equations near $u = 0$ are documented in [17].

Boundary conditions:

On $v = v_w$, $\psi = \psi_w$ and $n_+ = n_0$, $n_e = n_0$

On $v = \pi/2$, $\psi = 0$ and $n_+ = n_0$, $n_e = n_0$

On $u = 0$, $\partial\psi/\partial u = 0 = \partial n_{+,e}/\partial u$ — this is the axial symmetry condition, and, as $u \to \infty$, $\partial\psi/\partial u \to 0$, and $n_{+,e} \to n_0$. (8)

Initial conditions: The initial number density of electrons and ions, N_0, is non-zero due to the omni-present background radiation and has a value of 6×10^8 m^{-3} [18]: therefore,

$$n_{+,e} = n_0 \qquad \text{at} \quad t = 0. \quad (9)$$

The initial potential distribution is given by the solution to Laplace's equation in prolate spheroidal coordinates [17, pp. 165–167]:

$$\psi = \frac{\psi_w \ln[\tan v]}{\ln[\tan (v_w)]}. \quad (10)$$

III. NUMERICAL EXPERIMENTS

The three simultaneous, time dependent, second order, nonlinear partial differential equations, Eqs. (6) and (7) and a similar one for ions, are solved using a finite difference algorithm discussed below. Salient features of various numerical experiments are:

(1) Either implicit time integration or Crank–Nicolson procedure is used;

(2) Central differences are used for the discretization of diffusion terms;

(3) Either the upwind difference method or the central difference method is employed for the drift terms. In the upwind method [19, pp. 83–85], a combination of forward and backward differences is used for drift terms depending on the sign of the charge on the particle and the direction of the local component of electric field. The use of upwind differencing allows one to account for the drift of the positively and negatively charged particles in a direction appropriate with the sign of their charge in the local electric field. This is not always possible with central, forward, or backward differences alone;

(4) Where possible, the ionization and recombination terms are linearized with a negative slope to satisfy the "positive coefficient rule" [19, p. 38].

Since implict time differencing, the Crank–Nicolson procedure, and the central difference form of the diffusion terms are straightforward, they are not discussed here (refer to Patankar [19]). For the purpose of demonstration of the upwind differencing of the drift terms, we choose the v-direction drift term (third term on the LHS of Eq. (6)) in the electron number density equation. Using central differences for this term, first we have

$$\frac{\partial}{\partial v}\left[\sin v\, n_e \frac{\partial \psi}{\partial v}\right]\Bigg|_{i,j} = \frac{\sin(v+(\Delta v/2))\, n_e\, (\partial\psi/\partial v)|_{i,j+1/2}}{\Delta v} - \frac{\sin(v-(\Delta v/2))\, n_e\, (\partial\psi/\partial v)|_{i,j-1/2}}{\Delta v}. \quad (11)$$

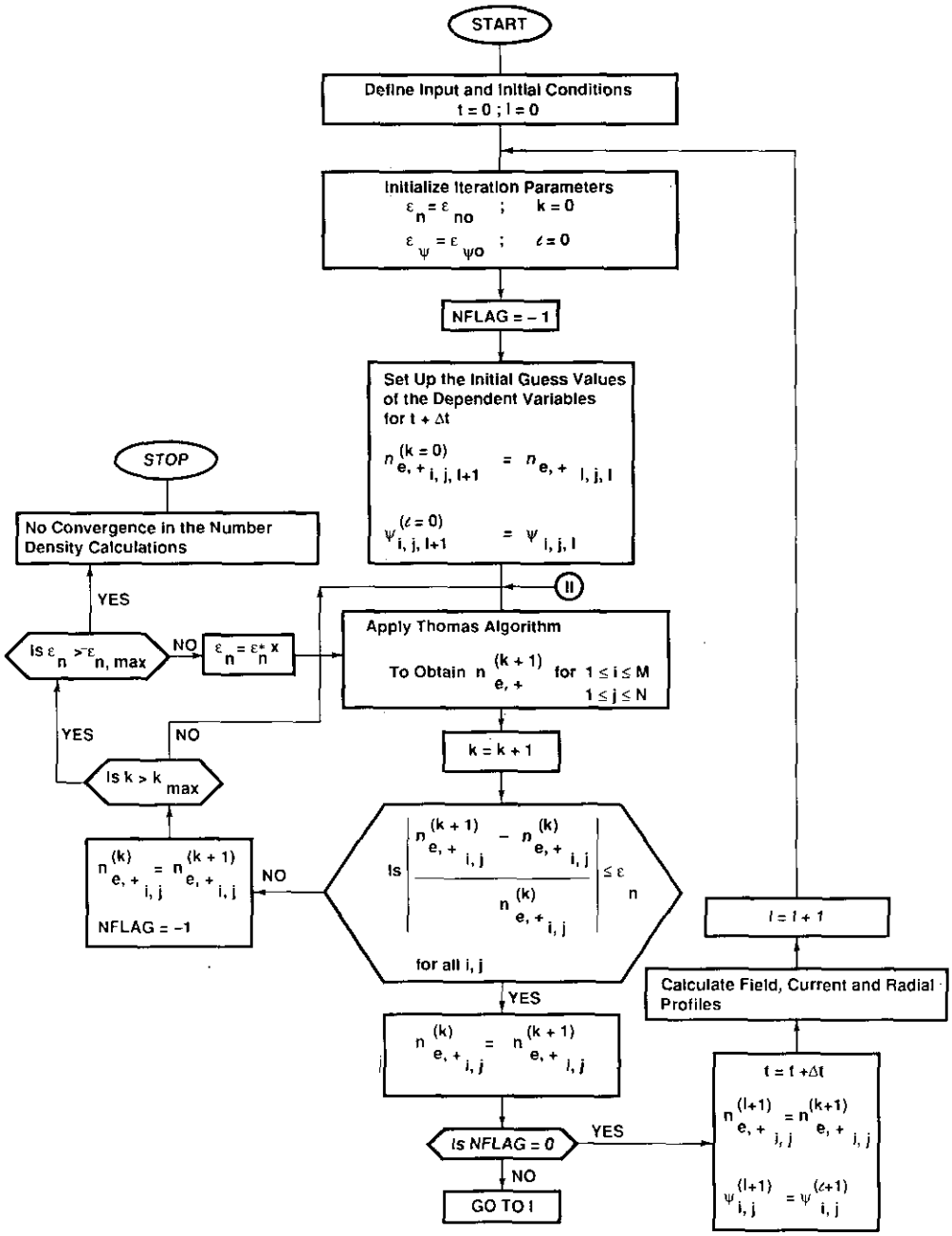

FIG. 2. Flow chart depicting the methodology of solution to the algebraic equations.

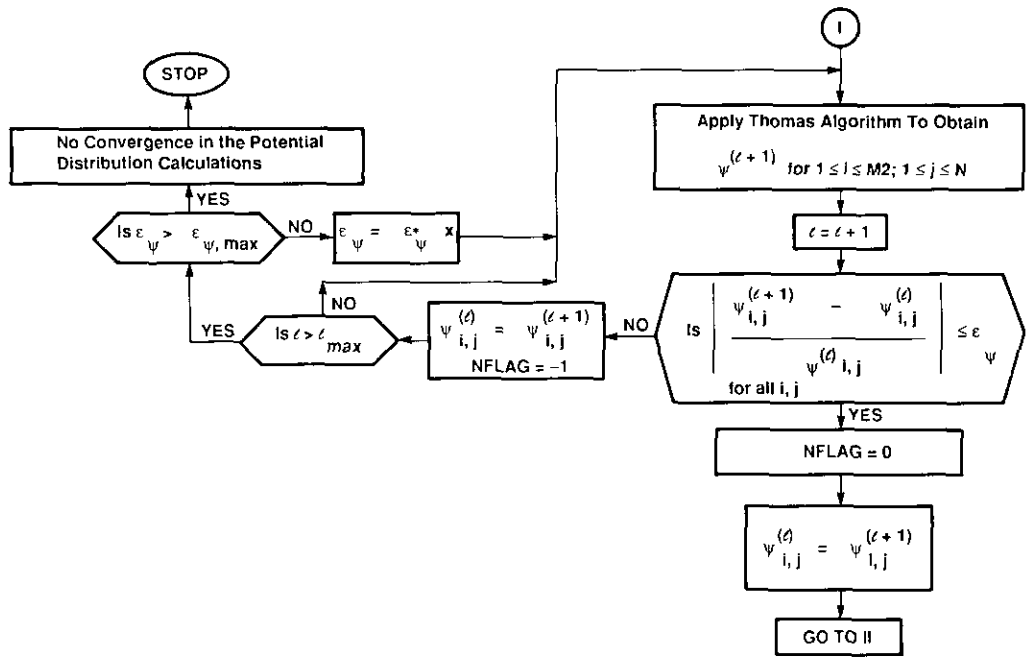

FIG. 2—*Continued*

In the above equation, i is the index in the u-direction and j is in the v-direction. The derivatives in Eq. (11) are evaluated at the $(l+1)$ "future" time level in the implicit method. In the Crank–Nicolson scheme, they are evaluated as an arithmetic mean of their values at the "current" time level (l), and at "future" time level $(l+1)$. $j \pm \frac{1}{2}$ are halfway between the grid points. In the evaluation of the terms on the RHS of Eq. (11), the value of n_e is assigned so that the electrons drift in the direction of $-E_v$ $(=\partial\psi/\partial v)$. Therefore, we have

$$n_e \left.\frac{\partial\psi}{\partial v}\right|_{i,j+1/2} = \left\| \left(\frac{\partial\psi}{\partial v}\right)_{i,j+1/2}, 0 \right\| n_{e_{i,j}} - \left\| -\left(\frac{\partial\psi}{\partial v}\right)_{i,j+1/2}, 0 \right\| n_{e_{i,j+1}}, \quad (12)$$

where

$$\|A, B\| = A \quad \text{if} \quad A > B$$
$$= B \quad \text{if} \quad B > A.$$

The derivatives of the potential in Eq. (12) are evaluated by central differences. The above procedure describes discretization for interior points of the solution domain. At the boundaries, where the boundary conditions of the first type are specified viz., at $v = v_w$ and $\pi/2$ (Eq. (8)), there is no need for discretization of the differential equations. On the discharge axis $(u = 0)$, limiting forms of the governing equations are derived first [17]. Finite difference approximations of these limiting forms of the equations are derived by the procedure described above by considering a fictitious point to the left of $u = 0$, located at a distance of $-\Delta u$. The unknown values of the variables at the fictitious point in the finite difference approximation are solved in terms of their values at points immediately to the right of the axis (located at Δu) by applying the symmetry conditions outlined in Eq. (8). Fictitious points are also used in the discretization of the differential equations at the outer boundary $(u \to u_\infty)$.

Central differences are used in discretizing the Poisson's equation for the potential, Eq. (7). The resulting algebraic equations for number densities as well as for potential may be cast in the form:

$$a_{i,j-1}\, x_{i,j-1} + a_{i,j}\, x_{i,j} + a_{i,j+1}\, x_{i,j+1} = b_{i,j} - a_{i-1,j}\, x^{(k+1)}_{i-1,j} - a_{i+1,j}\, x^{(k)}_{i+1,j}. \quad (13)$$

In this form the algebraic equations are suitable for solution by the line-by-line method using the tridiagonal (Thomas) algorithm. See Patankar [19].

III.1. *Solution of Non-linear Algebraic Equations*

The algebraic equations in Eq. (13) are solved by using the line-by-line method [19, pp. 64–66] along with the Thomas (tridiagonal) algorithm. In this problem ionization spreads from the wire $(v = v_w)$ towards the plane $(v = \pi/2)$ and from the axis $(u = 0)$ outwards towards the ambient

$(u \to \infty)$. For this reason the line-by-line method is swept one way in the u-direction—from the axis $(u = 0)$ outwards $(u \to \infty)$, instead of sweeping along the u- and v-directions alternately. In this way, the information at the wire, in the form of the recent values of the primitive variables in the numerical solution ($(k+1)$ terms on the right-hand side of Eq. (13)), is carried simultaneously to the plane at each u and from the axis outwards in the u-direction. This reduces the number of iterations in the line-by-line method. The flow chart depicting the solution methodology is shown in Fig. 2.

The presence of far diagonal terms, the nonlinear nature of the ionization and recombination terms, and the coupling of the species conservation equations with Poisson's equation, necessitates an iterative solution of the algebraic equations. We start with the solution known at time t (level l). A two-tier iteration scheme is used to solve the algebraic equations. In this iterative scheme, with a guessed potential distribution, convergence on the number densities, n_+ and n_e, is first obtained at time $t + \Delta t$ (level $l+1$). With these converged number density distributions, the potential distribution is updated by solving Poisson's equation. The current potential distribution is then employed in recalculating the number densities. This procedure is continued until the number densities and the potential are consistent with each other. Then, we advance to the next time level, viz., $l+2$.

Alternately, all three dependent variables might have been iterated at the same time level by simultaneously solving for all three variables combined, viz., $n_{e,+}$ and ψ, as opposed to splitting them into two groups—the number densities into one group and the potential into another. However, such an iterative scheme requires (approximately 30%) more computational time. Since the changes in the potential distribution during the earlier part of the transient are much smaller than the changes in the number densities, fewer iterations are required to achieve convergence for the potential. Moreover, the potential distribution at $t = 0$ is known analytically. If the iteration process combines the potential and the number densities, Poisson's equation is solved as many times as is required to obtain convergence on number densities, thereby requiring more computational time.

We have used a successive underrelaxation method to control the convergence of the algebraic equations. The relaxation parameter is varied during the transient, using a value of one at the beginning of the calculations and is reduced to about 0.2–0.3 during the period of steep rise in number densities. A small value of underrelaxation parameter keeps the numerical solution close to the previously converged solution during a period of rapid increase in number densities.

We begin the calculations at time $t = 0$ with a convergence criterion of 10^{-6} (0.0001%). The convergence criterion is defined as the *fractional* change in a quantity under consideration between two successive iterations, k and $k+1$. It may be noted that a value of 10^{-6} is very small for a convergence criterion and is rather stringent. As the transient progresses and the charged particle number densities increase rapidly, convergence cannot be obtained with 10^{-6} for a fixed number of iterations. At this point the convergence criterion is increased by a factor of two to 2×10^{-6} and the solution is continued until the next occurrence of convergence failure, at which time the convergence criterion is again increased by two to 4×10^{-6}. This process is continued and if the convergence criterion increases beyond 0.01 (i.e., 1%) the computations are terminated. Throughout this process the maximum number of iterations is kept constant. After some trials, we have used a maximum of 200 iterations for both number densities and for electrostatic potential.

III.2. *Radial Profiles and Current Calculations*

In order to obtain the radial number density profiles (in cylindrical coordinates), we transform and interpolate the results obtained in prolate spheroidal coordinates. In general, a radial line at a fixed axial location intersects the surfaces of constant u and v between the computational nodes. To arrive at radial profiles the results of the computation are linearly interplated in terms of arc lengths on the hyperboloidal and prolate spheroidal surfaces. The integrals in the calculations of current are evaluated by Simpson's rule. The derivatives at the electrodes are calculated by a three-point parabolic approximation so that they are second-order accurate. It is found that a two-point linear interpolation near the boundaries is too inaccurate to determine these derivatives.

IV. RESULTS AND DISCUSSION

The governing equations have been solved for a range of values of the applied voltage difference and for both positive and negative polarity of the wire. The computations have been performed on the Cray-X/MP-48 and IBM 3090. Since many variables are involved, extensive numerical experimentation has been carried out to ensure the accuracy and stability of the numerical solutions.

IV.1. *Initial Guess for Number Densities and Potential*

Two different types of initial guess values for the number densities are used to start the iterative scheme. They are:

(a) The converged solutions from the previous time step are the starting "guess" solutions, and

(b) The starting solution at the beginning of a new time step is evaluated from an analytical solution for the number

densities. This is possible if the diffusion and drift of charged particles is ignored.

Both of them converged to the same solution at each time step.

IV.2. *Renormalized Number Densities*

In order to explore the effect of roundoff, the number densities are renormalized by the initial number density, N_0, (rather than using N_R) so that the initial nondimensional number densities are equal to one and they are of order one or larger during this phase of the breakdown. Without such a renormalization, the number densities are initially of the magnitude of 10^{-8} and become of the order one or larger (approximately 1 to 100) as the discharge evolves (i.e., time progresses).

IV.3. *Renormalized Potential*

The potential distribution, at each time level, is calculated from Poisson's equation by solving it in three different ways:

(a) By normalizing the potential with kT'_∞/e and using the line-by-line method to solve Poisson's equation. With such a normalization the potential varies by nearly four decades from cathode to anode.

(b) By the use of the Gauss–Seidel iteration for the algebraic equations arising from Poisson's equation (with the same normalization as above) in place of the line-by-line method. It may be noted here that in a situation similar to this, Sundararajan and Ayyaswamy [20] have observed that a point-by-point (Gauss–Seidel) iteration is more appropriate as it does not propagate numerical errors as fast as the line-by-line method.

(c) By renormalizing the potential in Poisson's equation so that it is one (1) on the wire and zero (0) on the plane and then using the line-by-line method to solve the algebraic equations.

The agreement among the results of the above numerical experiments is satisfactory. However, the Gauss–Seidel method requires 2–4 times more iterations to arrive at the converged solution than the line-by-line method. There is excellent agreement between the results of these two iterative methods. We have used the line-by-line method along with the Thomas algorithm for the number densities and potential distribution in the two-dimensional study of electrical breakdown.

IV.4. *Choice of u_∞*

In our model, the solution domain extends to infinity in the u direction but, in the numerical solution, infinity is represented by a large, but finite number, u_∞. u_∞ is sufficiently large that the entire solution becomes insensitive to the variation of its numerical value. An appropriate choice of u_∞ also ensures that the derivatives of the number densities with respect to u tend to zero smoothly as $u \to u_\infty$. In this connection we note that the previous two-dimensional simulations [4, 6] have used experimentally deduced values of the discharge radius rather than determining it as a part of the solution and are not self-contained.

Computations have been performed with $u_\infty = 1.5$, 2, 2.5, 3, and 5 and the resulting density and potential distributions in the u direction have been compared. Figure 3 shows one such comparison with $u_\infty = 2.5$ and 5 at a potential difference of -2500 V. For $u_\infty < 2.5$, u-derivatives of the dependent variables do not tend to zero smoothly as $u \to \infty$. For this reason, u_∞ is set to 2.5 in the computations for all of the voltages reported in [15, 17].

IV.5. *Different Outer Boundaries for Densities and Potential*

When the charge separation in the solution domain becomes significant, its effects may extend beyond the outer boundary used for the number densities. The computations show that charge separation near the axis appears to be important and the solution boundary for computing the potential distribution may have to extend beyond $u_\infty = 2.5$. For this reason, we have employed $u_\infty = 2.5$ as the outer boundary for number densities and $u_\infty = 5$ for the potential. This increases the outer radius of the solution domain from $6L$ (with $u_\infty = 2.5$) to $80L$ (with $u_\infty = 5$), where L is the gap length on the discharge axis. Beyond $u_\infty = 2.5$, $n_e = n_+ = n_0$,

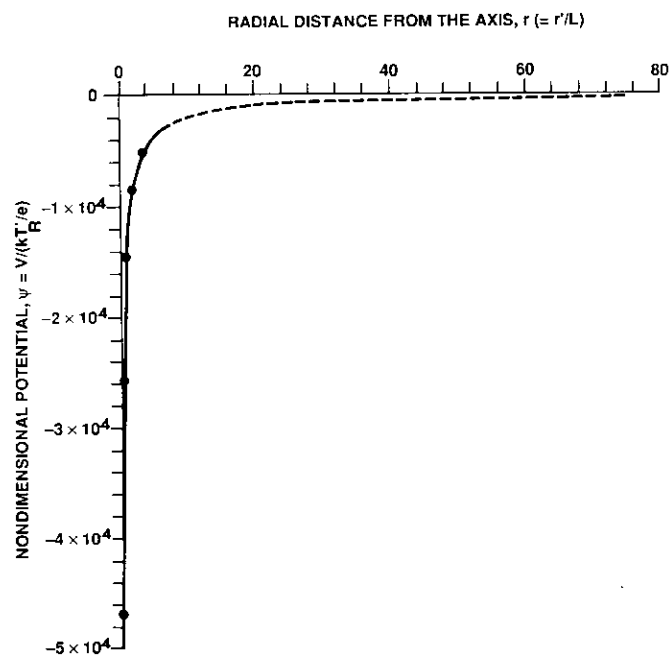

FIG. 3. Comparison between the radial profiles of potential distribution at $t = 0.795$ with $u_\infty = 2.5$ and 5, respectively. Wire is at -2500 V. Legend: solid line → $u_\infty = 2.5$; dashed line → $u_\infty = 5.0$.

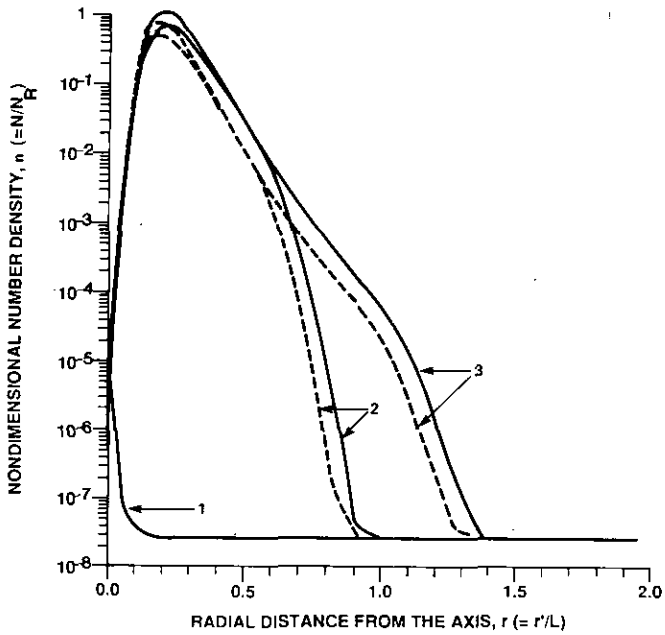

FIG. 4. Comparison between the radial profiles of electron number density at different times during the breakdown, with the wire at -2500 V, with: A. $u_\infty = 2.5$ for densities and for potential distribution; B. $u_\infty = 2.5$ for densities and 5 for potential distribution. Legend: solid line → (A); dashed line → (B). 1. $t = 7.5 \times 10^{-5}$; 2. $t = 0.295$; 3. $t = 0.795$.

and the net charge density in Poisson's equation is set to zero. Davies *et al.* [4] have used such a spatial grid in a two-dimensional axisymmetric simulation of breakdown for a parallel plate geometry (in cylindrical coordinates). Figure 4 shows a comparison between the radial profiles of electron number density computed with $u_\infty = 2.5$ for both the number densities and potential (dashed lines) and the same profiles computed with $u_{\infty,n} = 2.5$ for number densities and with $u_{\infty,\psi} = 5$ for the potential distribution (solid lines). The agreement between the results is not good and point to the need for the use of different solution boundaries for the number densities and the potential. A similar trend is also noted for ion density profiles. We have used different boundaries for n and ψ in our computations. Larger values than 2.5 and 5 for $u_{\infty,n}$ and $u_{\infty,\psi}$, respectively, are not necessary. Moreover, a smaller value of u_∞ requires less computer memory during the execution of the program.

TABLE II

Typical Δt vs. t

t	Δt
$0-10^{-4}$	1×10^{-5}
$>10^{-4}-10^{-3}$	5×10^{-5}
$>0.001-0.01$	5×10^{-4}
$>0.01-1.8$	5×10^{-3}
$>1.8-2.0$	1×10^{-3}
>2.0	5×10^{-3}

IV.6. *Grid Size and Time Step*

A uniform grid has been employed for the spatial coordinates, u and v, and a variable time step, Δt, is used. Computations have been performed with Δu in the range 0.125 to 0.025 and with five to 400 divisions along the v-direction. From these experiments we have arrived at a value of 0.05 for Δu and 200 divisions in the v-direction. Δu is kept the same for the solution domain for number densities and potential. Typically a value of 10^{-5} is used for Δt at the beginning of the simulation and it is increased gradually as time, t, increases to accommodate numerical accuracy and to capture important physical phenomena. A satisfactory variation of Δt vs. t is obtained after a few trials. A typical Δt vs. t used in most of the computations is shown in Table II. Several combinations of Δt, Δu, and Δv have been attempted before arriving at a satisfactory set of values for each ΔV investigated. This is done to strike a balance between guiding the solution through without missing the avalanche in number densities and keeping the total number of time steps to a minimum.

IV.7. *Other Numerical Methods*

In the course of this investigation, we have observed that when the wire is negatively biased with respect to the plane, peaks in the radial number density profiles occurred away from the discharge axis as the discharge evolved, i.e.,

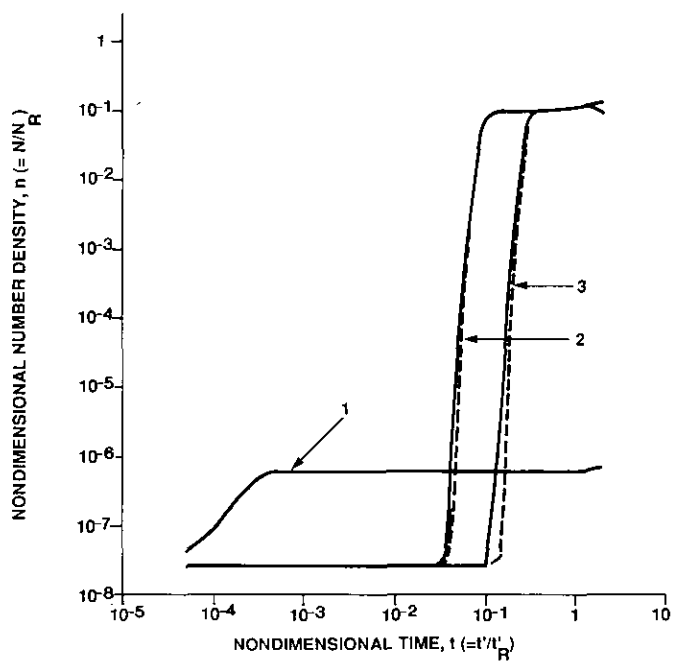

FIG. 5. Comparison between the results of computation with the implicit and Crank–Nicolson methods of integration. Temporal development of electron densities at several locations along the discharge axis ($u = 0$). Legend: solid lines → implicit method; dashed lines → Crank–Nicolson method; 1. $Z = 0.99$; 2. $Z = 0.80$; 3. $Z = 0.67$; 4. $Z = 0.36$.

as the time increased. An explanation of the physics of the phenomena is given in [15, 17]. To ensure that the phenomenon is not an artifact of the numerical solution, we have solved the problem using other finite difference schemes. They have included the use of combinations of upwind and central differences, with implicit and Crank–Nicolson time integration methods.

As noted earlier, central differences can be used for both drift and diffusion terms. Instead of implicit time integration, Crank–Nicolson time integration can be used as it is also unconditionally stable. However, the Crank–Nicolson method requires more computational time and storage as the spatial derivatives and source terms in the equations are arithmetic averages of their values at the present and future times, i.e., at time levels l and $l+1$. Different combinations of finite differencing of time and drift terms give rise to the following algorithms: (1) upwind and implicit methods, (2) central differences and implicit methods, (3) upwind and Crank–Nicolson methods, and (4) central differences and Crank–Nicolson methods. We note here that for all these cases central differences have been employed for the diffusion terms. We have performed calculations for the first three cases only. Use of central differences for drift terms violates the positive coefficient rule [19, p. 37] and, with increased time, the numerical solutions develop oscillations. Otherwise the results show the same general trends as with the upwind method. The results obtained by using the implicit and Crank–Nicolson methods of time integration, along with the upwind

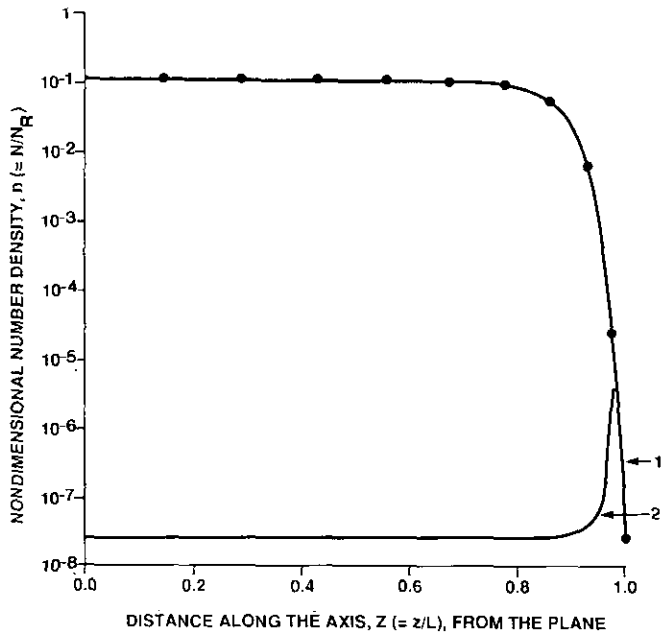

FIG. 6. Comparison between the results of computation with the implicit and Crank–Nicolson methods. Shown here is the development of the electron number density profiles on the axis of the discharge, with the wire at -2500 V. Legend: solid lines → implicit method; dashed lines → Crank–Nicolson method; 1. $t = 7.5 \times 10^{-5}$; 2. $t = 0.795$.

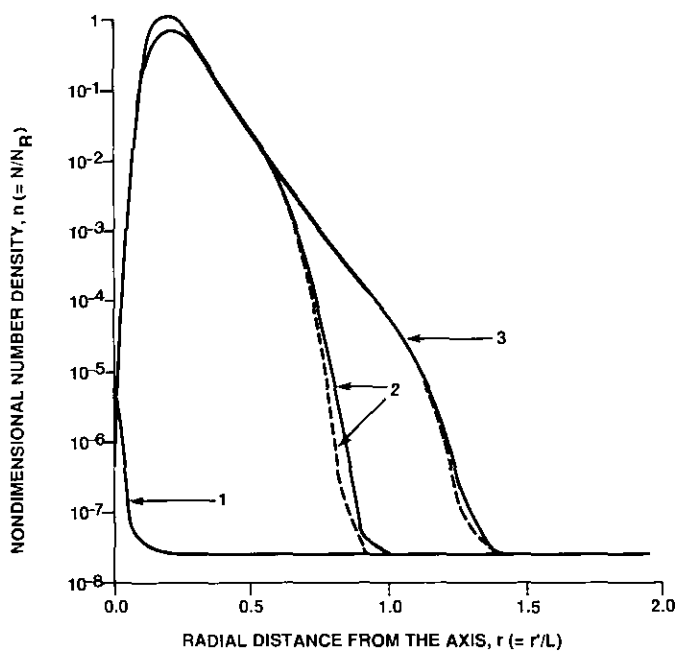

FIG. 7. Comparison between the results of computation with the implicit and Crank–Nicolson methods. Shown here is the development of the radial profiles of the electron number density, with the wire at -2500 V. Legend: solid lines → implicit method; dashed lines → Crank–Nicolson method; 1. $t = 7.5 \times 10^{-5}$; 2. $t = 0.295$; 3. $t = 0.795$.

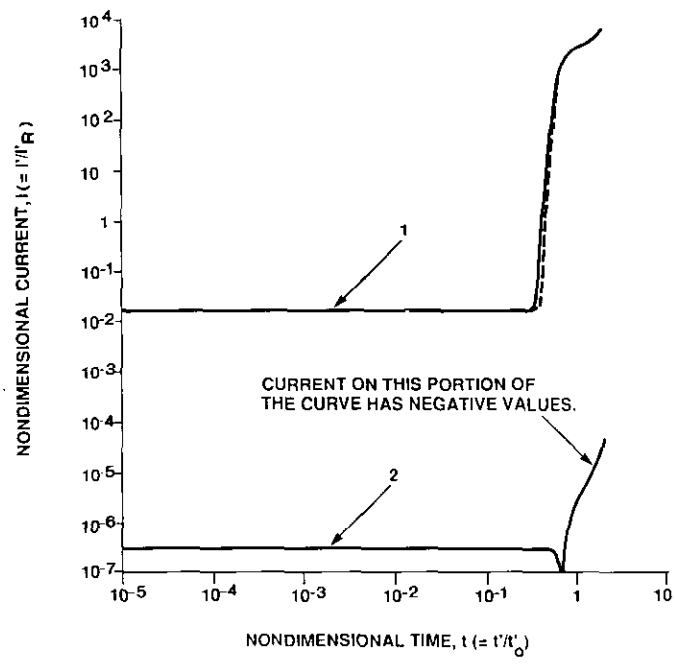

FIG. 8. Comparison between the results of computation with the implicit and Crank–Nicolson methods. Electron and ion current growth at the wire are shown here, for a potential difference of -2500 V. Legend: solid lines → implicit method; dashed lines → Crank–Nicolson method; 1. electron current; 2. ion current.

method, are compared for the temporal growth of electron densities (Fig. 5), the axial and radial profiles of electron densities (Fig. 6 and 7, respectively), and for the current growth (Fig. 8). The agreement may be considered to be very good. Such comparisons have also been made for ion densities and for the potential distribution with similar conclusions. Since the Crank–Nicolson method requires more computing time and memory, we conclude that the implicit method is preferred.

A combination of central differences and Crank–Nicolson has not been investigated as this combination has given rise to numerical oscillations in the solution. Our attempts at using explicit time integration have been unsuccessful due to the problems arising out of numerical instability of the algorithm and time step restrictions.

IV.8. *Effect of Artificial Diffusion and False Scaling*

Early studies on the numerical solutions of fluid flow employed central difference schemes (CDS) to represent the convection terms. CDS gives rise to numerical oscillations at high Reynolds number. To circumvent this difficulty, an upwind method (UDS) has been employed. Later it is recognized that UDS results in artificial diffusion and false scaling [21–23]. But, it does not suffer from the numerical instabilities associated with the CDS.

In this study, computations have also been performed using central differences for the drift terms and some of the observations have been presented in the previous section. The occurrence of peaks in the charged particle densities is of particular interest to our study [15, 17].

The results of computations with the CDS and UDS for the drift terms are compared in Fig. 9 for the electron number density growth on the axis. It may be noted that the CDS develops oscillations (curve 1 in Fig. 9). During the initial time, when there are no oscillations, the agreement between the results with CDS and UDS schemes is good. The numerical oscillations in the CDS increase in amplitude with increase in time and ionization. The ion density curves, shown in Fig. 10, also show similar trends and the amplitude of oscillations is smaller at any given time.

The radial profiles of the electron and ion densities are compared from the CDS and UDS computations in Figs. 11 and 12, respectively. At initial times, both methods show peaks in the electron density on the discharge axis (curve 1 in Fig. 11) and at later times both the schemes show the peaks moving away from the axis (curve 2 in Fig. 11) for a negatively biased wire. For a positively biased wire, the peaks in number densities remain on the discharge axis [15, 17]. From this, we may conclude that the occurrence of peaks away from the axis, for a negatively biased wire, is not an artifact of the upwind method. Computations for the CDS have not been carried out beyond $t = 5 \times 10^{-4}$ as the numerical oscillations are too large.

IV.9. *Electrical Breakdown with Negative Ions*

In electronegative gases, like air and oxygen, experimental evidence points to the formation of negative ions.

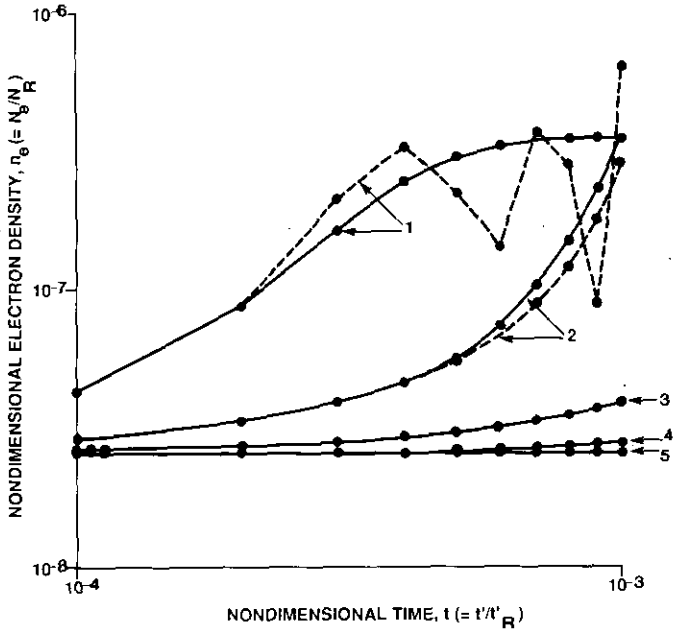

FIG. 9. Comparison between the results of computation with the UDS and the CDS for the drift terms. Temporal development of the electron densities on the discharge axis with the wire at -1500 V.

Note. Solid lines, UDS; dashed lines, CDS. 1. $Z = 0.995$; 2. $Z = 0.98$; 3. $Z = 0.96$; 4. $Z = 0.93$; 5. $Z = 0.9$.

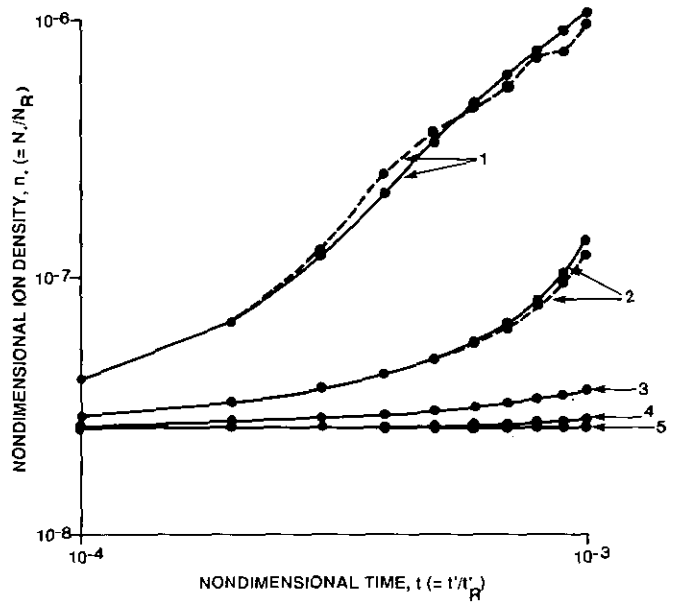

FIG. 10. Comparison between the results of computation with the UDS and the CDS for the drift terms. Temporal development of the ion densities on the discharge axis with the wire at -1500 V.

Note. Solid lines, UDS; dashed lines, CDS. 1. $Z = 0.995$; 2. $Z = 0.98$; 3. $Z = 0.96$; 4. $Z = 0.93$; 5. $Z = 0.9$.

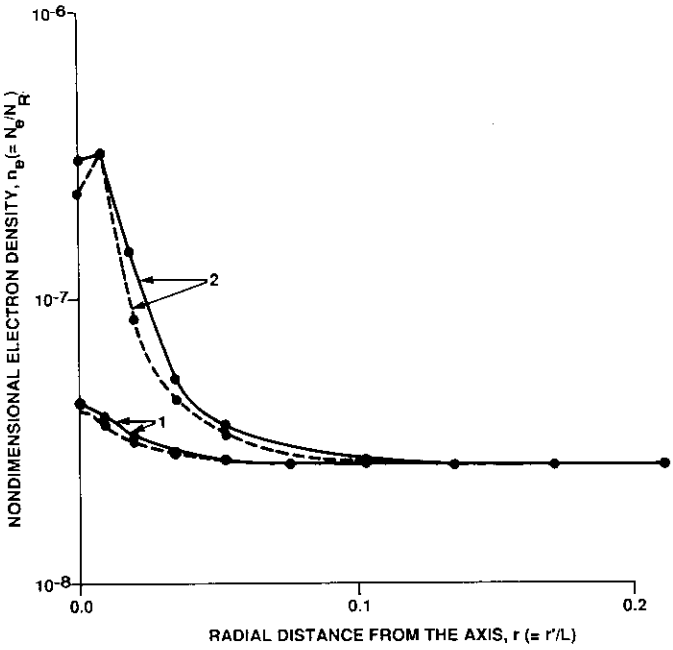

FIG. 11. Comparison between the results of computation with the UDS and the CDS for the drift terms. Development of the radial profiles of electron densities with the wire at -1500 V; $Z = 0.99$.

Note. Solid lines, UDS; dashed lines, CDS. 1. $t = 10^{-4}$; 2. $t = 5 \times 10^{-4}$.

Negative ions of oxygen, O^- and O_2^-, have been identified as playing an important role in the development of the discharge in air [17, Chap. 3]. Two species of negative ions are described by two specie conservation equations, in addition to the equations describing the evolution of electrons, positive ions, and the electrostatic potential. Thus, the total number of equations to be solved increases to five. However, the algorithm remains the same. In the iterative solution of the non-linear algebraic equations, the equations for the negative ion densities are included in the number density block (refer to Fig. 2) and are iterated with electron and ion densities. In this iteration block, the following solution sequence is implemented: electrons, ions, and, negative ions. This sequence follows the relative importance of the species in their effect on the growth of the discharge. No additional problems are encountered in the computations with the negative ions. The results are discussed in [17, Chap. 3].

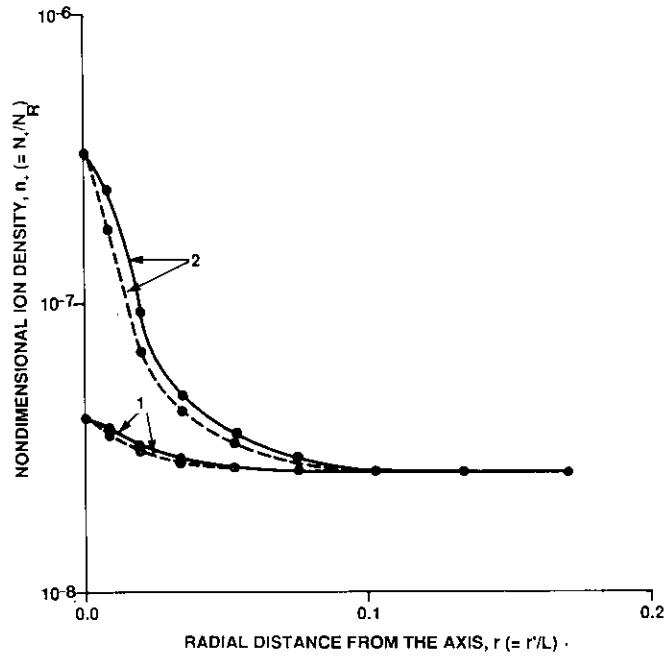

FIG. 12. Comparison between the results of computation with the UDS and the CDS for the drift terms. Development of the radial profiles of ion densities with the wire at -1500 V; $Z = 0.99$.

Note. Solid lines, UDS; dashed lines, CDS. 1. $t = 10^{-4}$; 2. $t = 5 \times 10^{-4}$.

V. SUMMARY AND CONCLUSIONS

In this paper, we have developed a finite difference solution to the two-dimensional, axisymmetric problem of electrical breakdown in a non-uniform gap. Upwind differences for the drift terms, central differences for the diffusion terms, and implicit time integration have been employed. Additionally, central differences for the drift terms and Crank–Nicolson time integration are investigated. The methods have been subjected to extensive numerical experimentation. From this study we conclude that a finite difference algorithm with implicit time integration and the upwind method for drift terms yield accurate results until the time that the quasi-neutral regions develop in the bulk and sheaths appear adjacent to the electrodes. We have also found that the use of central differences for the drift terms leads to oscillations in the numerical solutions. Results with implicit and Crank–Nicolson time integration methods are in good agreement. Since the implicit method requires less computing time and memory, it is to be preferred. Even though the method is demonstrated for a prolate spheroidal coordinate system, it is equally applicable to other right-hand coordinate systems. The algorithm is not coordinate system dependent. The algorithm is extended to the breakdown model of air with negative ions, in which case the total number of governing equations increases from three to five.

APPENDIX: NOMENCLATURE

a	semi-focal distance (m).
A_i	constant in the equation relating Townsend's first ionization coefficient to the ratio E'/p (m/N).
B_i	constant in the equation relating Townsend's first ionization coefficient to the ratio E'/p (m/N).
$\mathbf{B}_i$	nondimensional form of B_i ($= B_i p/E'_R$).
$\mathbf{C}_1$	constant in Eq. (6).
$\mathbf{C}_2$	constant in Eq. (6).
d	twice the radius of curvature at the tip of the hyperboloidal wire (m).

$\mathbf{E}$	dimensional electric field intensity (V/m).
$\mathbf{E}'$	dimensionless electric field intensity.
e	charge on a single electron (Coulomb).
F	a dimensionless parameter in Eq. (6) with a suitable subscript.
g	statistical weight.
k	Boltzmann constant (J/K); iteration parameter for number densities.
L	gap length on the discharge axis (m).
l	present time level, t (values of all the primitive dependent variables are known).
$l+1$	future time level, $t+\Delta t$, (values of all the primitive dependent variables are unknown).
N	dimensional number density (m^{-3});
N_R	number density used in normalizing the charged particle densities, (m^{-3}) [$=kT_\infty \varepsilon_0/(e^2 d^2)$].
n	nondimensional number density (appropriately subscripted)[$=N/N_R$].
P	volumetric production terms (m^{-3}/s).
R	volumetric recombination terms (m^{-3}/s).
p	pressure (Pa).
T'	dimensional temperature (K).
T	dimensionless temperature [$=T'/T'_\infty$].
t'	dimensional time (s).
t	nondimensional time [$=t'/t'_R$].
t'_R	time used in normalization (s) ($=1/(A_i p \mu_e E'_R)$).
Δt	time step.
u, v, ϕ	prolate spheroidal coordinates.
Δu	grid spacing in u direction.
V	dimensional electrostatic potential (V).
Δv	grid spacing in v direction.
x, y, z	Cartesian coordinates.

Greek symbols

ε_0	permittivity of free space (farad/m).
Ψ	dimensionless potential [$=eV/kT'_\infty$]
Γ	particle current density (m^{-2}/s).
μ	mobility of a charged particle ($m^2/V\,s$).

Subscripts

e	electrons.
n	pertaining to the number density; neutral particles.
w	wire.
Ψ	pertaining to the potential.
$+$	ions.
∞	ambient.

ACKNOWLEDGMENTS

This work was supported by the National Science Foundation under Grant DMC 8513128 and by the Commonwealth of Pennsylvania through the Benjamin Franklin Partnership (Grant 06.500.NU). Computations were made possible by NSF Supercomputer Grants DMC 0000000/8513128 and ECS 0000000/8515068 at the Pittsburgh Supercomputing Center. We would like to thank Dr. K. Himasekhar of Advanced CAE Technology, Inc., of Ithaca, NY for his comments on the manuscript.

REFERENCES

1. J. M. Meek and J. D. Craggs (Eds.), *Electrical Breakdown in Gases* Wiley Series in Plasma Physics (Wiley, New York, 1978).
2. A. J. Davies, C. J. Evans, and F. Llewellyn-Jones, *Proc. R. Soc. London A* **281**, 164 (1964).
3. A. J. Davies, C. S. Davies, and C. J. Evans, *Proc. IEE* **118**, 816 (1971).
4. A. J. Davies, C. J. Evans, and P. Townsend, *Proc. IEE* **124**, 179 (1977).
5. K. Yoshida and H. Tagashira, *J. Phys. D: Appl. Phys.* **9**, 435 (1976).
6. A. J. Davies, C. J. Evans, and P. M. Woodison, in *Proceedings of the International Symposium on Gaseous Dielectrics, Knoxville, TN, 1978*, edited by L. G. Christophorou, p. 84.
7. A. L. Ward, *Phys. Rev. A* **138**, 1357 (1965).
8. R. Morrow, *J. Comput. Phys.* **43**, 1 (1981).
9. R. Morrow, *J. Comput. Phys.* **46** (3), 454 (1982).
10. R. Morrow and L. E. Cram, *J. Comput. Phys.* **57**, 129 (1985).
11. J. P. Boris and D. L. Book, *J. Comput. Phys.* **43**, 38 (1973).
12. C. D. Munz, *J. Comput. Phys.* **77**, 18 (1988).
13. J. P. Novak and R. Bartnikas, *J. Appl. Phys.* **62**, 3605 (1987).
14. A. J. Davies, *Proc. IEE* **133** (Pt. A, No. 4), 217 (1986).
15. K. Ramakrishna, I. M. Cohen, and P. S. Ayyaswamy, *J. Appl. Phys.* **65** (1), 41 (1989).
16. N. N. Lebedev, *Special Functions and their Applications*, translated by R. A. Silverman (Dover, New York, 1972).
17. K. Ramakrishna, Ph.D. dissertation, Dept. of Mech. Eng. and Appl. Mechanics, University of Pennsylvania, Philadelphia, PA, 1989 (unpublished).
18. R. G. Fleagle and J. A. Businger, *An Introduction to Atmospheric Physics*, Int. Geophysics Series, Vol. 25, 2nd ed. (Academic Press, New York, 1980), pp. 135, 150.
19. S. V. Patankar, *Numerical Heat Transfer and Fluid Flow* (Hemisphere, Washington, DC, 1980).
20. T. Sundararajan and P. S. Ayyaswamy, *Numer. Heat Transfer* **8**, 689 (1985).
21. G. de Vahl Davis and G. D. Mallinson, *Computers and Fluids* **4**, 29 (1976).
22. M. Joseph, *Comput. Methods Appl. Mech. Eng.* **39**, 107 (1983).
23. J. C. Strikwerda, *J. Comput. Phys.* **47**, 303 (1982).